Rapid Communications

High spectral resolution of GaAs/AlAs phononic cavities by subharmonic resonant pump-probe excitation

Camille Lagoin, Bernard Perrin, Paola Atkinson, and Daniel Garcia-Sanchez*

Sorbonne Universités, UPMC Université Paris 06, CNRS-UMR 7588, Institut des NanoSciences de Paris, F-75005 Paris, France

(Received 21 September 2018; published 11 February 2019)

We present here precise measurements of the resonance frequency, lifetime, and shape of confined acoustic modes in the tens of GHz regime in GaAs/AlAs superlattice planar and micropillar cavities at low temperatures (∼20 K). The subharmonic resonant pump-probe technique, where the repetition rate of the pump laser is tuned to a subharmonic of the cavity resonance to maximize the amplitude of the acoustic resonance, has been used in combination with a Sagnac interferometer technique for high sensitivity (∼10 fm) to the surface displacement. The cavity fundamental mode at ∼20 GHz and the higher-order cavity harmonics up to ∼180 GHz have been clearly resolved. Mechanical Q values up to 2.7×10^4 have been measured in a planar superlattice, and the direct spatial mapping of confined acoustic modes in a superlattice micropillar cavity has been demonstrated. The Q-frequency product obtained is $\sim 5 \times 10^{14}$, demonstrating the suitability of these superlattice cavities for optomechanical applications.

DOI: 10.1103/PhysRevB.99.060101

The field of optomechanics studies the interaction of an optical cavity with a mechanical resonator. Recently, optomechanical devices have attracted great interest for their potential in nonlinear optics [1] and for the demonstration of macroscopic quantum mechanics [2–4].

Superlattice micropillars have emerged as a promising choice for optomechanical experiments because they exhibit high acoustic resonance frequencies and large optomechanical coupling factors [5,6] which are a requirement for nonlinear optomechanics. In addition, superlattice micropillar cavities have been used to prepare single photon sources [7,8] and to demonstrate polariton lasing [9]. The optical properties of the micropillars have been extensively studied; high-quality-factor optical cavities have been fabricated [10,11] and optical mode shapes have been imaged [12].

Although preliminary theoretical [6,13] and experimental [5,14] studies of the acoustic modes have been realized, the full phononic characterization of confined modes in micropillars in the GHz regime poses significant experimental challenges, and standard optomechanical measurement techniques such as homodyne interferometry have not yet been successful.

Conversely, the pump-probe technique is very well suited for the detection of high-frequency acoustic phenomena, ranging from a few GHz up to 10 THz [5,15–19]. Recently, this technique has been used to study micropillar cavities with a fundamental frequency ∼19 GHz and quality factor ∼1000 at room temperature [5,14].

In this Rapid Communication, we have carried out pump-probe measurements of the acoustic transmission coefficient of planar and micropillar GaAs/AlAs superlattice cavities at low temperature (20 K). In contrast to room-temperature measurements, where the phonon-phonon interaction considerably reduces the mechanical quality factor, at low temperature the quality factor of the superlattice cavities is not limited by phonon absorption of the bulk material [20]. An improvement of the phonon lifetime of crystalline materials such as GaAs by several orders of magnitude at low temperature has been observed [20–23].

However, the spectral resolution of standard pump-probe experiments is limited by the repetition rate of the pulsed laser oscillator and/or the delay line and is insufficient to measure high intrinsic quality factors. We have overcome this frequency resolution limit by using a subharmonic excitation technique [24] where the repetition rate of the laser pulse is tuned through resonance with a subharmonic of the acoustic mode.

The technique presented here is a passive characterization of the acoustic cavity. Opaque 60-nm Al films deposited on the bottom and top surfaces of the samples [see Fig. 1(a)] provide an effective transfer mechanism for acoustic excitation and detection [17] and suppress any photoelastic interaction between the optical beams and the superlattice cavity. In addition, the transmission configuration used here suppresses any cross-talk between the pump and probe.

A femtosecond pulse train excitation is generated by a mode-locked Ti:sapphire laser with a tunable repetition rate $79.6 < f_{\mathrm{rep}} < 80.2$ MHz driven by a rf frequency generator. The pump pulse is focused on the back side of the sample which generates a broadband acoustic pulse that propagates through the substrate and the acoustic superlattice cavity. The pulse can be reflected several times by the back side and the front side of the sample, giving rise to a series of echoes. The travel time can be defined as the time that an echo takes to complete a round trip. When the acoustic pulse reaches the front-side surface it generates a displacement that is probed using a Sagnac interferometer [25] [see Fig. 1(a)] which has a higher sensitivity than the reflectometric technique in the 16–20 GHz low-frequency range [15]. The two probe pulses

*daniel.garcia-sanchez@insp.upmc.fr

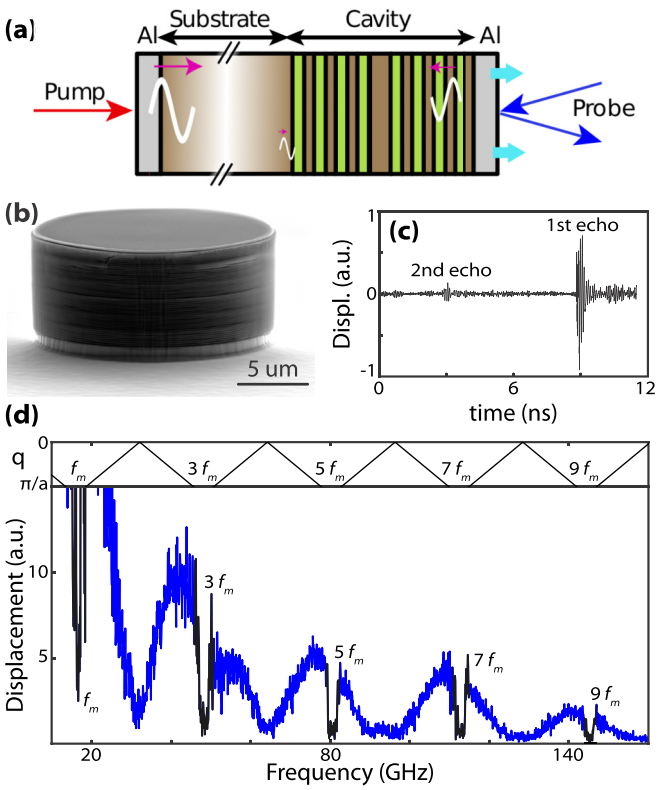

FIG. 1. (a) Device and measurement scheme. (b) Scanning electron microscopy picture of a 16-μm-diam micropillar cavity. (c) Time trace of a 16-μm-diam micropillar cavity obtained by pump-probe measurement. The second echo arrives before the first echo due to folding. (d) Corresponding acoustic spectrum. The schematic band structure can be found in the top part of the figure. The band gaps around the first, third, fifth, seventh, and ninth harmonics can be seen in the measurement.

of the interferometer reach the sample surface with a time difference built to be equal to one half of the acoustic mode period $1/2f_{\mathrm{m}}$; this doubles the signal at the phononic resonance frequency. The pump is modulated at $f_{\mathrm{mod}} \approx 1$ MHz and a lock-in amplifier is used to improve the signal-to-noise ratio.

The superlattice cavities discussed here are formed by two distributed Bragg reflector (DBR) mirrors consisting of 15, 20, or 25 repeats of GaAs/AlAs bilayers on either side of a $\lambda/2$ GaAs cavity that has been grown on a nominally 370-μm-thick GaAs (100) wafer by molecular beam epitaxy (MBE). The micropillars have been etched by inductively coupled plasma etching [see Fig. 1(b)]. This etching process results in very smooth and straight sidewalls [10]. The GaAs/AlAs layer thicknesses, and theoretically expected values of the cavity frequency, quality factor, and amplitude lifetime of the three samples discussed here are given in Table I.

Figure 1(c) shows the time trace of the acoustic displacement, measured by the Sagnac interferometer, of a 16-μm-diam micropillar from sample M20. The second echo (at 3 ns) arrives before the first echo (9 ns) because of the time trace fold inside the measurement window. This time arrival difference and the repetition rate can be used to determine the pulse travel time with great accuracy.

TABLE I. Characteristics of the samples: thicknesses of the GaAs and AlAs mirror layers. Expected theoretical properties: resonance frequency f_m^{th}, quality factor Q_{th}, and amplitude lifetime τ_{th}.

Name	GaAs/AlAs (nm)	f_m^{th} (GHz)	Q_{th}	τ_{th} (ns)
P15: planar	59.7/71.3	19.9	2.3×10^3	37
M20: micropillars	75.1/88.7	15.9	1.5×10^4	300
P25: planar	60.0/70.1	20.4	10^5	10^4

The Fourier transform of the time trace gives the corresponding acoustic spectrum [see Fig. 1(d)]. Our pump-probe experimental setup allows all the phononic gaps of the superlattice from 16 GHz up to 180 GHz to be unequivocally identified. These correspond to the theoretical Brillouin zone boundary gaps shown in the top part of Fig. 1(d). In our experiments, the spectral resolution is limited to 87 MHz by the 11.5-ns delay line. As a result, our pump-probe technique, if the laser repetition rate is fixed, does not allow a resonance at 20 GHz with a quality factor higher than 100 to be resolved.

To extract the quality factor by varying the laser repetition rate, we have to take into account the cumulative effect of the pump pulse train excitation [26] in the pump-probe scheme. The quadrature in-phase and out-of-phase outputs of the synchronous detection are given by $X(\tau)$ and $Y(\tau)$, where τ is the probe to pump delay time. The complex output signals $s^{\pm}(\tau) = X(\tau) \pm iY(\tau)$ are given by

$$s^{\pm}(\tau) = \sum_{p=0}^{+\infty} \varphi(\tau + p/f_{\mathrm{rep}}) e^{\pm i2\pi f_{\mathrm{mod}}(\tau + p/f_{\mathrm{rep}})}, \qquad (1)$$

where $\varphi(\tau)$ is the displacement due to a single pump pulse. When the frequency is close to the acoustic resonance of the cavity, the displacement $\varphi(\tau)$ can be modeled by a damped harmonic oscillator motion $\varphi(\tau > 0) \propto e^{-\tau/\tau_m} \cos(2\pi f_m \tau)$, where f_m is the acoustic resonance frequency and τ_m the acoustic amplitude lifetime. Then Eq. (1) becomes

$$s^{\pm}(\tau) \propto \frac{e^{-\tau/\tau_m} e^{2i\pi f^{\pm}\tau}}{1 - e^{-1/(\tau_m f_{\mathrm{rep}})} e^{2i\pi f^{\pm}/f_{\mathrm{rep}}}}, \qquad (2)$$

where $f^{\pm} \equiv (f_m \pm f_{\mathrm{mod}})$.

The power spectrum $|S^{\pm}|^2(f)$ shows a maximum at $f^{\pm}$ corresponding to the cavity acoustic resonance. The amplitude of $|S^{\pm}|^2(f^{\pm})$ depends on the repetition rate and has a Lorentzian shape centered around $f_{\mathrm{rep}}^n = (f_m \pm f_{\mathrm{mod}})/n$, with n a positive integer. The subharmonic excitation is resonant when $f^{\pm}/f_{\mathrm{rep}} = n$ and antiresonant when $f^{\pm}/f_{\mathrm{rep}} = n \pm 1/2$. The full width at half maximum (FWHM) of the Lorentzian resonance is given by $\Delta f = \frac{1}{\pi n \tau_m}$ and can be used to calculate the lifetime τ_m and the quality factor $Q = \pi f_m \tau_m$ of the acoustic cavity.

The lifetime of the acoustic resonance cavities that we have studied is larger than the laser repetition period $\sim$1/80 MHz. As a result, the acoustic resonance is not observed unless a specific repetition rate is chosen [see Fig. 2(a)].

If the repetition rate is $f_{\mathrm{m}}/f_{\mathrm{rep}} \approx 245 + 1/2$, the spectrum amplitude at resonance is completely suppressed because the pulse train excitation is antiresonant with the phononic cavity

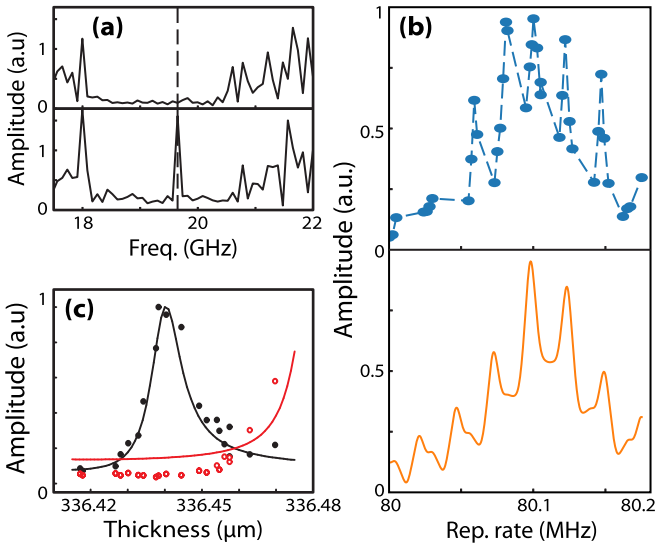

FIG. 2. (a) Zoom in of the acoustic spectrum around the fundamental cavity mode. The upper curve corresponds to an antiresonant excitation with $f_{\rm rep} = 79.990$ MHz and $f^+/f_{\rm rep} \simeq 245 + 1/2$. The lower curve corresponds to a resonant excitation with $f_{\rm rep} = 80.130$ MHz and $f^+/f_{\rm rep} \simeq 245$. (b) Acoustic resonance amplitude as a function of the laser repetition rate. Measurement in the upper curve and fit in the lower curve. (c) Acoustic resonance amplitude as a function of the substrate thickness (proportional to the travel time). The experimental data (dots) and fit (line) are shown for the two signals resonant at $f_m + f_{\rm mod}$ in black and $f_m - f_{\rm mod}$ in red.

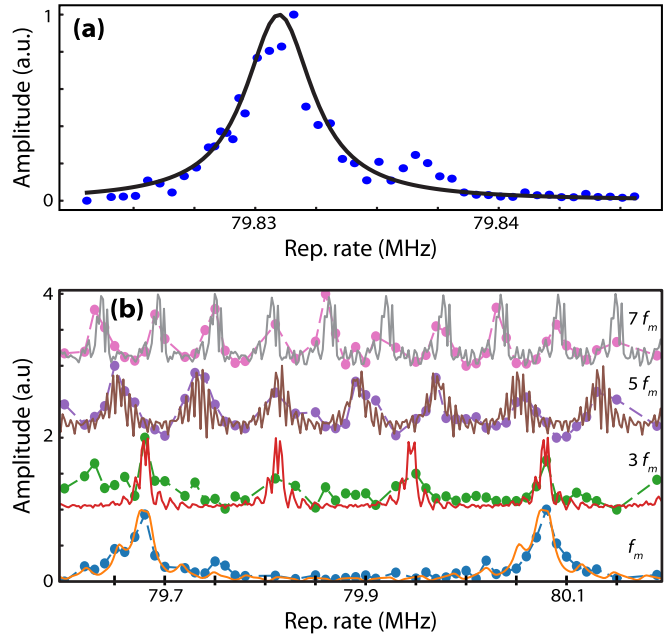

FIG. 3. (a) Acoustic resonance amplitude as a function of the laser repetition rate for a 25-bilayer planar device. (b) Measured amplitude and fit of the fundamental acoustic mode of a 16-μm-diam pillar, $f_{\rm m}$ (16.0 GHz), and its odd harmonics, $3f_{\rm m}$ (48 GHz), $5f_{\rm m}$ (80 GHz), $7f_{\rm m}$ (112 GHz).

[upper panel of Fig. 2(a)]. On the other hand, if the repetition rate is $f_{\rm m}/f_{\rm rep} \approx 245$, as in the lower panel of Fig. 2(a), the resonance amplitude is maximum because the pulse train excitation is resonant with the phononic cavity: This is the subharmonic resonant excitation condition.

Figure 2(b) shows the amplitude of the cavity mode of the planar sample P15 versus the laser repetition rate. A series of narrow peaks is superimposed over a broader peak. This is due to the fact that the sample effectively consists of two coupled cavities: the superlattice cavity and the substrate which is itself an acoustic Fabry-Pérot cavity. The series of sharp peaks corresponds to the substrate cavity and the spacing between these peaks depends on the substrate thickness which is proportional to the echo travel time (for this device, 158 ns). The envelope of the peaks corresponds to the superlattice cavity resonance and the width is inversely proportional to the cavity quality factor. The transmission factor of the coupled cavities has been calculated using a one dimensional (1D) transfer matrix method [27]; diffraction losses in the substrate, accounting for the anisotropy of GaAs, have been included in the calculation.

In order to test the high sensitivity of the subharmonic technique, the laser repetition rate was set at 80.100 MHz, corresponding to the maximum of a sharp peak related to the substrate echo [see Fig. 2(b)], and the sample was moved over a distance of 0.5 mm. Since the substrate thickness is not homogeneous across the wafer, the echoes' travel time depends on the position on the sample, and as a result, the series of sharp peaks from Fig. 2(b) shifts in repetition rate.

The effect of varying the thickness of the substrate cavity on the vibrational displacement amplitude at a fixed repetition rate is shown in Fig. 2(c). The two curves correspond to the two signals resonant at $f^{\pm}$. As the sharp echo peak width (1.3 MHz) is smaller than twice the modulation frequency (3.2 MHz), we can resolve the two resonances and observe that here the f^- peak is maximum while the f^+ is minimum.

This shows that if the superlattice cavity resonance is broad, acoustic echoes can have a significant effect on the acoustic mode response and care should be taken if measurements are carried out at a fixed repetition rate at different positions on a sample. To reduce the magnitude of the acoustic echoes we focus the pump beam more tightly on the sample back side to ensure that the acoustic wave diffracts more when propagating back and forth inside the sample. The echo peaks also play less of a role when studying higher quality factor cavities and in small diameter pillars.

Figure 3(a) shows the spectrum of a 25-bilayer DBR planar superlattice cavity from sample P25. We measure the waist of the probe and pump optical beams which are respectively 2 and 4.8 μm. From the optical waist of the pump focalized on the back side, we can evaluate the waist of the acoustic excitation incident on the superlattice cavity taking into account the diffraction during the propagation inside the substrate and the GaAs anisotropy around the (100) axis. We find a waist of 14.3 μm at 20 GHz.

The linewidth of the 25 repeat superlattice cavity is in the same order of magnitude as the free spectral range of the substrate cavity; as a result, we do not observe the series of sharp peaks that we observed in Fig. 2(b).

This allows the quality factor of the superlattice cavity to be measured with good precision $Q_{\rm meas} = 27\,200$ (corresponding

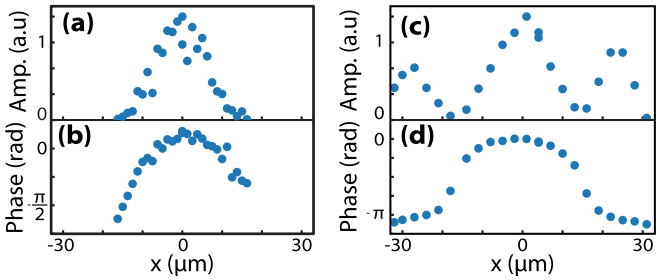

FIG. 4. Mode profile of a 32-μm-diam micropillar: (a) amplitude and (b) phase. Mode profile of a 64-μm-diam micropillar: (c) amplitude and (d) phase.

to a lifetime $\tau_m = 413$ ns) which is approximately four times smaller than the theoretical quality factor $Q_{\text{th}} = 10^5$. At 20 K, the intrinsic damping of GaAs cannot explain this difference [20]. The reduction in Q is instead likely to be due to random thickness fluctuations of the MBE-grown DBR mirrors [16]. We would like to note that we have observed as well a reduction in the optical Q of these superlattice cavities.

Figure 3(b) shows the fundamental mode, the third, the fifth, and the seventh harmonics resonance amplitudes of a 16-μm-diam micropillar from sample M20 versus the laser repetition rate. The waist of the acoustic excitation at 16 GHz incident on the superlattice cavity is estimated to be 17 μm. Owing to the tunability of the repetition rate of our laser and its stability (10 Hz), this technique allows the detection and study of acoustic resonances with frequencies in the range 10–100 GHz. Indeed, in Fig. 3(b) for the fundamental mode curve, we can see two peaks which correspond to the resonant excitation of two different subharmonics and we observe as expected more subharmonic resonances for the higher-order modes. We extracted a quality factor of $Q_{\text{th}} = 7000$ ($\tau_m = 135$ ns) for the fundamental 16-GHz mode which is roughly two times smaller than the theoretical quality factor, again probably due to fluctuations in the mirror layer thicknesses.

Our technique also allows the mode profile of the micropillars to be investigated. We scanned the micropillar surface by moving the probe beam along one direction of the micropillar. Figures 4(a) and 4(b) show the amplitude and the phase of the resonance of a 32-μm-diam micropillar. As expected for a longitudinal acoustic mode, the amplitude and the phase are axisymmetric. We have also investigated the acoustic mode profile of a 64-μm micropillar cavity [see Figs. 4(c) and 4(d)]. We observed several amplitude maxima which could be due to a hybrid mode and will be thoroughly studied in future works.

In conclusion, we have demonstrated that the subharmonic resonant technique allows the frequency resolution limit of the standard pump-probe measurement to be overcome and allows cavity mode lifetimes much larger than the time interval between two laser pulses to be measured. We were able to measure a quality factor in the order of 2.7×10^4 for a mode frequency as high as 20 GHz which gives a $Q - f$ product of 5.0×10^{14} at 20 K, comparable to state-of-the-art optomechanical photonic crystals [28] which have recently been used to verify the nonclassical nature of a phonon state [3] and to demonstrate quantum entanglement between two micromechanical oscillators [2]. It should be noted that the Q factors measured here were not limited by the measurement resolution and that the technique presented here should allow $Q - f$ products as large as 2×10^{16} to be measured. In addition, the measurement resolution of ~5 kHz permitted shifts in the resonance frequency of different pillars to be clearly resolved–corresponding to a sensitivity to small changes in the cavity thickness of 0.3 nm due to a gradient in the growth thickness across the substrate. Finally, we have demonstrated that this high-resolution technique allows the mode profile of the acoustic mode to be imaged, opening up the possibility of testing theoretical models and tailoring acoustic modes to maximize the optomechanical coupling of superlattice micropillars in the future.

This work project was supported by the Agence Nationale de la Recherche and the Idex Sorbonne Universités under Contract No. ANR-11-IDEX-0004-02, through the MATISSE program.

[1] A. H. Safavi-Naeini, S. Groblacher, J. T. Hill, J. Chan, M. Aspelmeyer, and O. Painter, Nature (London) **500**, 185 (2013).
[2] R. Riedinger, A. Wallucks, I. Marinković, C. Löschnauer, M. Aspelmeyer, S. Hong, and S. Gröblacher, Nature (London) **556**, 473 (2018).
[3] S. Hong, R. Riedinger, I. Marinković, A. Wallucks, S. G. Hofer, R. A. Norte, M. Aspelmeyer, and S. Gröblacher, Science **358**, 203 (2017).
[4] W. Marshall, C. Simon, R. Penrose, and D. Bouwmeester, Phys. Rev. Lett. **91**, 130401 (2003).
[5] A. Fainstein, N. D. Lanzillotti-Kimura, B. Jusserand, and B. Perrin, Phys. Rev. Lett. **110**, 037403 (2013).
[6] D. Garcia-Sanchez, S. Déleglise, J.-L. Thomas, P. Atkinson, C. Lagoin, and B. Perrin, Phys. Rev. A **94**, 033813 (2016).
[7] N. Somaschi, V. Giesz, L. De Santis, J. C. Loredo, M. P. Almeida, G. Hornecker, S. L. Portalupi, T. Grange, C. Antón, J. Demory, C. Gómez, I. Sagnes, N. D. Lanzillotti-Kimura, A. Lemaítre, A. Auffeves, A. G. White, L. Lanco, and P. Senellart, Nat. Photonics **10**, 340 (2016).
[8] X. Ding, Y. He, Z.-C. Duan, N. Gregersen, M.-C. Chen, S. Unsleber, S. Maier, C. Schneider, M. Kamp, S. Höfling, C.-Y. Lu, and J.-W. Pan, Phys. Rev. Lett. **116**, 020401 (2016).
[9] D. Bajoni, P. Senellart, E. Wertz, I. Sagnes, A. Miard, A. Lemaître, and J. Bloch, Phys. Rev. Lett. **100**, 047401 (2008).
[10] C. Arnold, V. Loo, A. Lemaître, I. Sagnes, O. Krebs, P. Voisin, P. Senellart, and L. Lanco, Appl. Phys. Lett. **100**, 111111 (2012).
[11] S. Reitzenstein, C. Hofmann, A. Gorbunov, M. Strauß, S. H. Kwon, C. Schneider, A. Löffler, S. Höfling, M. Kamp, and A. Forchel, Appl. Phys. Lett. **90**, 251109 (2007).

[12] G. Ctistis, A. Hartsuiker, E. van der Pol, J. Claudon, W. L. Vos, and J.-M. Gérard, Phys. Rev. B **82**, 195330 (2010).
[13] F. Lamberti, Q. Yao, L. Lanco, D. T. Nguyen, M. Esmann, A. Fainstein, P. Sesin, S. Anguiano, V. Villafañe, A. Bruchhausen, P. Senellart, I. Favero, and N. D. Lanzillotti-Kimura, Opt. Express **25**, 24437 (2017).
[14] S. Anguiano, A. E. Bruchhausen, B. Jusserand, I. Favero, F. R. Lamberti, L. Lanco, I. Sagnes, A. Lemaître, N. D. Lanzillotti-Kimura, P. Senellart, and A. Fainstein, Phys. Rev. Lett. **118**, 263901 (2017).
[15] B. Perrin, C. Rossignol, B. Bonello, and J.-C. Jeannet, Physica B **263**, 571 (1999).
[16] G. Rozas, M. F. Pascual Winter, B. Jusserand, A. Fainstein, B. Perrin, E. Semenova, and A. Lemaitre, Phys. Rev. Lett. **102**, 015502 (2009).
[17] A. Huynh, N. D. Lanzillotti-Kimura, B. Jusserand, B. Perrin, A. Fainstein, M. F. Pascual-Winter, E. Peronne, and A. Lemaître, Phys. Rev. Lett. **97**, 115502 (2006).
[18] A. Amziane, L. Belliard, F. Decremps, and B. Perrin, Phys. Rev. B **83**, 014102 (2011).
[19] T. Bienville, J. Robillard, L. Belliard, I. Roch-Jeune, A. Devos, and B. Perrin, Ultrasonics **44**, Suppl. 1, e1289 (2006).
[20] R. Legrand, A. Huynh, B. Jusserand, B. Perrin, and A. Lemaître, Phys. Rev. B **93**, 184304 (2016).
[21] M. Goryachev, D. L. Creedon, E. N. Ivanov, S. Galliou, R. Bourquin, and M. E. Tobar, Appl. Phys. Lett. **100**, 243504 (2012).
[22] S. Galliou, J. Imbaud, M. Goryachev, R. Bourquin, and P. Abbe, Appl. Phys. Lett. **98**, 091911 (2011).
[23] W. Chen, H. Maris, Z. Wasilewski, and S. Tamura, Philos. Mag. B **70**, 687 (1994).
[24] A. Bruchhausen, R. Gebs, F. Hudert, D. Issenmann, G. Klatt, A. Bartels, O. Schecker, R. Waitz, A. Erbe, E. Scheer, J.-R. Huntzinger, A. Mlayah, and T. Dekorsy, Phys. Rev. Lett. **106**, 077401 (2011).
[25] E. Péronne, N. Chuecos, L. Thevenard, and B. Perrin, Phys. Rev. B **95**, 064306 (2017).
[26] B. Perrin, in *Microscale and Nanoscale Heat Transfer*, edited by S. Volz, Topics in Applied Physics Vol. 107 (Springer, Berlin, 2007), pp. 333–359.
[27] C. Rossignol, B. Perrin, B. Bonello, P. Djemia, P. Moch, and H. Hurdequint, Phys. Rev. B **70**, 094102 (2004).
[28] A. G. Krause, J. T. Hill, M. Ludwig, A. H. Safavi-Naeini, J. Chan, F. Marquardt, and O. Painter, Phys. Rev. Lett. **115**, 233601 (2015).